Compressive Feedback-Based Motion Control for Nanomanipulation—Theory and Applications

Bo Song, *Student Member, IEEE*, Jianguo Zhao, *Student Member, IEEE*, Ning Xi, *Fellow, IEEE*, Hongzhi Chen, *Student Member, IEEE*, King Wai Chiu Lai, *Member, IEEE*, Ruiguo Yang, *Student Member, IEEE*, and Liangliang Chen

***Abstract*—Conventional scanning probe microscopy (SPM)-based nanomanipulations always have to face scanner accuracy problems such as hysteresis, nonlinearity, and thermal drift. Although some scanners consist of internal position sensors, the sensitivity is not high enough to monitor high-resolution nanomanipulations. Additionally, once the scan size decreases to a nanolevel such as less than 100 nm, the noise brought by sensors is large enough to affect the performance of the closed-loop motion control system. In this paper, a non-vector space control strategy based on compressive feedback is proposed in order to improve the accuracy of SPM-based nanomanipulations. In this approach, local images (or compressive data) are used as both the reference input and feedback for a non-vector space closed-loop controller which considers the local image (or compressive data) as a set. The controller is designed in non-vector space, and it requires no prior information on features or landmarks which are widely used in traditional visual servoing. In this paper, the atomic force microscopy is used as an example of SPM to implement the non-vector space control strategy for nanomanipulations. The motivation of designing such a non-vector space controller is to solve the accuracy problem in nanomanipulation. Without this technique, the SPM-based nanomanipulations, such as nanomeasurement and nanosurgery, are difficult to conduct, with accuracy controlled under several nanometers. In order to illustrate the contributions and potential applications of this non-vector controller, at the end of this paper, an application of carbon nanotube local electrical property characterization based on a non-vector space motion control is shown to clearly verify the concept. Compared with other research in the local electrical property characterization, the non-vector space controller can ensure that the measurement accuracy (position error) is controlled within a few nanometers, which also ensures the reliability of measurement results. Additionally, this non-vector space control method can be implemented into any kind of SPM to realize a real-time control for nanomanipulation such as nanofabrication and nanoassembly.**

***Index Terms*—Compressive feedback, nanomanipulation, nanorobotics, non-vector space.**

Manuscript received March 28, 2013; revised September 6, 2013; accepted November 7, 2013. Date of publication December 19, 2013; date of current version February 3, 2014. This paper was recommended for publication by Editor B. J. Nelson upon evaluation of the reviewers' comments. This work is partially supported by the National Science Foundation under Grant IIS-0713346 and Grant DMI-0500372; the Office of Naval Research under Grant N00014-04-1-0799 and Grant N00014-07-1-0935; and the National Institutes of Health under Grant R43 GM084520.

B. Song, J. Zhao, H. Chen, R. Yang, and L. Chen are with the Department of Electrical and Computer Engineering, Michigan State University, East Lansing, MI 48824 USA (e-mail: songbo@msu.edu; zhaojia1@msu.edu; chenhon5@msu.edu; yangruig@msu.edu; chenlia5@msu.edu).

N. Xi is with the Department of Electrical and Computer Engineering, Michigan State University, East Lansing, MI 48824 USA, and also with the Department of Mechanical and Biomedical Engineering, Kowloon, Hong Kong (e-mail: xin@egr.msu.edu).

K. W. C. Lai is with the Department of Electrical and Computer Engineering, Michigan State University, East Lansing, MI 48824 USA, and also with the Department of Mechanical and Biomedical Engineering, Kowloon, Hong Kong (e-mail: kinglai@cityu.edu.hk).

Color versions of one or more of the figures in this paper are available online at http://ieeexplore.ieee.org.

Digital Object Identifier 10.1109/TRO.2013.2291619

I. Introduction

THE nanoworld has been revolutionized by recent advances in technology, which enable imaging, manipulation, and measurement at the nano and molecular levels. Targeted nanoparticle imaging and manipulation have introduced nanotechnology to the biomedicine, material science, and physics studies. Laboratory-level testing and experiments of nanoscale require instruments that can provide nanoscale imaging and operation. As one of the centerpieces in nanotechnology, scanning probe microscopy (SPM) is a suitable candidate for such needs as it could scan and manipulate nanoparticles or single molecules at a nanoscale. SPMs such as scanning tunneling microscopy (STM) and atomic force microscopy (AFM) have been frequently used to image and manipulate nanomatters [1]–[3]. Usually, this kind of microscopy is equipped with a probe which has a very sharp tip (tip apex is approximately 10 nm or less) which can delicately scan on top of the sample surface to get the topography image. Besides imaging, the sharp tip can be considered as an end effector of the nanorobot which is capable of manipulating nanoobjects and modifying sample surfaces [4].

The accuracy of SPM imaging and manipulation highly depends on the accurate motion control of the probe (which is equipped at the end of the scanner). Although the piezoelectric tube scanner which is widely used in SPM has many advantages such as high response frequency, it still has several accuracy issues such as hysteresis, nonlinearity [5], and thermal drift [6]. These disadvantages might be acceptable for imaging but not for manipulation. The nanomanipulation system must have reliable and accurate motion control ability to precisely manipulate particles at a nanoscale. In order to improve these nonlinearity and thermal drift, models and sensors are introduced.

Typical compensation models, such as the Preisach method [7], which includes a feed-forward controller to solve hysteresis, can be used to solve the nonlinearity. It cannot, however, reduce the online error because of lacking feedback. Apart from the models, displacement sensors have been placed in SPMs to provide feedback. However, the precision of the closed-loop scanner has been limited by the performance of these sensors

(such as the strain gauge [8], the capacitive sensor [9], and the optical sensor [10]).

However, sensors have several drawbacks which need to be solved. First, sensors usually increase the system noise. Second, the displacement measured by sensors is the output of the piezo-tube, which is not the exact position of the probe tip since the cantilever of the probe might be bending during nanomanipulations.

In order to design a system which can solve the issue, how to get accurate motion control without introducing extra noise, we do not use extra sensors for generating the SPM scanner position feedback. Instead of sensors, the SPM images are used as both the reference input and the feedback to generate a closed-loop control system for tip motion control in the nanomanipulation system [11]. Apparently, it is a typical visual servo problem [12]. In visual servoing, images are used for locating a feature or landmark associated with coordinates transformation, allowing the visual servoing system to get the position or velocity feedback for the closed-loop system. The system does not need sensors to monitor the movement. However, the performance of conventional visual servoing heavily depends on feature extractions. Good features may not be easy to find and may be changed during manipulation [13]. Some researchers also studied visual servoing without the feature extraction process. Collewet and Marchand used the similarity of two images to define the mutual information which was used to design a controller [14]. Dame and Marchand used the completed image intensities as a feature vector to perform feedback control [15]. Although these methods work well, the approach in this paper is fundamentally different from them. In this approach, the image is considered as a set in non-vector space (there is no order to each element in the set), which is the advantage through which the random compressive data can be used as the feedback (detailed in Section IV). Moreover, vector space visual servo still needs accurate calibration which is difficult at a nanoscale.

In this paper, a novel control strategy was developed by utilizing the feedback/compressive feedback produced by images/compressive data which further improved our previous work [11]. Because the image or compressive feedback is a set, not a vector, the terminology *non-vector space control* is used. Additionally, the feedback can be a complete local image or partial image that can be considered as compressive data, which is the terminology *compressive feedback*. Inside this control system, both the controller and feedback are designed in the non-vector space for tip motion control to conduct SPM-based nanomanipulation (as shown in Fig. 1). Three crucial steps are essential for the control strategy: 1) Design a non-vector space controller in which the local image is used directly as the feedback. 2) Use compressive scanning to compress the sample and reconstruct a local image. Compressive sensing is introduced here to reduce the scanning time to increase the feedback rate. 3) Replace the complete feedback (local image) with compressed data directly to generate a compressive feedback (as shown in Fig. 1). In this step, we designed a non-vector space controller based on compressive feedback. After compressive scanning, it is not necessary to recover the local image that costs extra time on calculation. The compressive data obtained

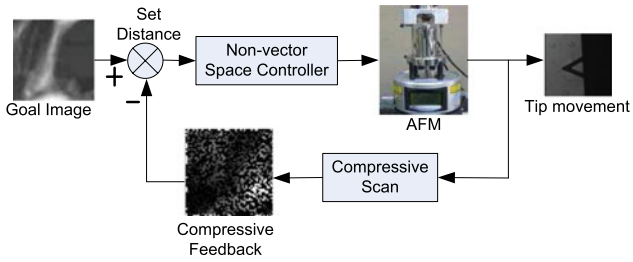

Fig. 1. Control diagram of the non-vector space control system with compressive feedback (with AFM as an example).

by compressive scanning is used directly as the feedback. In such a case, the controller must ensure the stability when the compressed data are used as the feedback of the closed-loop control. In this paper, AFM is used as a specific example to illuminate how a non-vector space controller works.

A number of potential applications of a non-vector space control are easily identified because of its accurate motion control at a nanoscale. It enables SPMs to conduct complicated nanomanipulations and nanomeasurements which were difficult or impossible to perform with traditional nanomanipulation methods. For example, SPMs have been proposed to study the local conductance of nanomaterials by employing a conductive probe as a movable electrode to conduct local conductance measurements. However, only a few attempts have been made because of the lack of accurate position control. In order to characterize the local electrical properties, spatial measurement resolution should be controlled within a few nanometers. It is difficult or even impossible prior to the development of a non-vector space control. A non-vector space control can conduct precise SPM tip motion control to accurately reach each measurement point which leads to reliable measurement results. In the last section of this paper, we present an AFM-based nanomanipulation application: carbon nanotube local conductivity characterization using a non-vector space control to illustrate the contribution of this new control strategy to explore the nanoworld.

II. Non-Vector Space Control Based on Local Complete Image

A non-vector space control strategy based on a local image is proposed in this section. A local image is obtained by performing a local scan, which only samples a small area of interest. It reduces sampling time so that an acceptable feedback rate is achievable [16].

In traditional visual servoing, features are first extracted from the image followed by a controller which is designed to reduce the position error between the desired and current vectors of features to zero [12]. Traditional visual servoing relies on feature extraction. In most visual servoing literatures, several fiducial markers are used for features so that the tracking of them can be easily achieved [13].

Different from the aforementioned traditional servoing methods, we developed a featureless method that directly uses the image intensity information. First, this method considers the image as a set. Second, we define the difference between sets

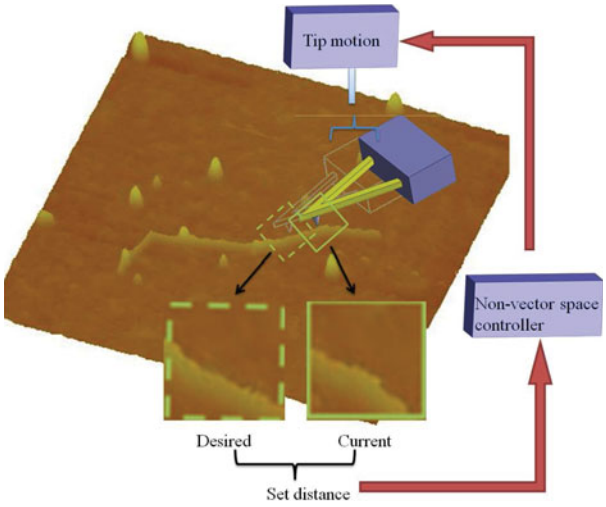

Fig. 2. Basic working approach of a non-vector space control.

as the error between the desired and current image sets. Finally, a non-vector space controller is designed to converge the difference to zero [17]. It should be noted that other featureless methods also exist, including the kernel-based method [18], the sum-of-square-difference method [19], and the entropy-based method [20]; however, the non-vector space control approach is fundamentally different from them. Although the controllers design in aforementioned applications were performed in the condition of featureless, the dynamics models are still in vector space. It brought difficulties in the design and theoretical analysis of the control systems. In our approach, both the dynamics model and the controller design are in non-vector space.

The basic non-vector space control strategy is shown in Fig. 2. First, a large area of interest is scanned by SPM. Then, a small image patch is chosen as the desired image (inside the large area SPM image). Then, the tip starts the local scanning to obtain a current image. According to the two sets corresponding to the desired image and current image, the non-vector space controller calculates the moving direction and speed for the SPM tip. Through updating current images, eventually the desired image matches the current image. In this way, the tip can be steered to the desired position for manipulation. This strategy is completely different from current visual servoing methodology. Although images are involved in the feedback in the conventional visual servoing, the image is used for recognizing features or landmarks in order to obtain the position information. In a non-vector space control system, images are directly used for reference input and state feedback without explicitly computing the position. Some other methods such as optical flow [21] could also be used in visual servoing. However, since optical flow methodology works in vector space, it requires time consuming delicate calibration before use, which is a drawback in the nanoworld.

In order to design such a control system (mentioned above), two fundamental issues need to be solved: how to define a difference (distance) in non-vector space and how to build a dynamic model in non-vector space. The non-vector space controller is based on the set, and if we want to solve these issues, mutation analysis should be used to formulate the dynamics model in non-vector space.

A. Basic of Mutation Analysis

Mutation analysis describes the dynamics of the sets. Take images as an example; the set used in non-vector space is defined as follows: Consider an $n \times n$ pixels image A, where $A = [a_{ij}], 1 \le i \le n, 1 \le j \le n$ and its set form X is defined as $X = \{[1, 1, a_{11}]^T, [1, 2, a_{12}]^T, \ldots, [i, j, a_{ij}]^T, \ldots, [n, n, a_{nn}]^T\}$. In order to formulate the difference between two sets, the set distance should be defined. Any set distance $d(X, Y)$ between sets X and Y must satisfy the following three conditions [22]:

1) Nonnegative: $d(X, Y) > 0$ if X is not the same with Y; $d(X, X) = 0$;
2) Symmetry: $d(Y, X) = d(X, Y)$;
3) Triangular Inequality: $d(X, Z) \le d(X, Y) + d(Y, Z)$ for any other set Z.

Any set distance which satisfies these three conditions could be applied in a non-vector space control system. In this paper, the Hausdorff distance is used as an example to discuss the controller design and stabilization problem.

Given a finite set of points $P \subset \mathbb{R}^n$, the set distance between the set P and a point $x \in \mathbb{R}^n$ is $d_P(x) = \min_{y \in P} \|y - x\|$. The projection from x to P is denoted as $\Pi_P(x) = \{y \in P : \|y - x\| = d_P(x)\}$. The Hausdorff distance between two sets P and Q is defined as

$$dh(P, Q) = \max\Big\{ \max_{p \in P} \min_{q \in Q} \|p - q\|, \max_{q \in Q} \min_{p \in P} \|q - p\| \Big\}. \tag{1}$$

Following are some extra definitions for the set dynamics. A tube $K(t) \subset \mathbb{R}^n$ is a mapping: $K: \mathbb{R}^+ \mapsto 2^{\mathbb{R}^n}$, where $2^{\mathbb{R}^n}$ is the powerset of $\mathbb{R}^n$. For example, in the case when gray scale images are the sets, the tube is the surface evolution with respect to time in the 3-D space. Define $\varphi: E \mapsto \mathbb{R}^n$ with $E \subset \mathbb{R}^n$ as a bounded Lipschitz function. The set of all such functions is denoted as $\mathrm{BL}(E, \mathbb{R}^n)$. Then, the transition for $\varphi \in \mathrm{BL}(E, \mathbb{R}^n)$ is defined as

$$T_\varphi(t, K_0) = \{x(t) : \dot{x} = \varphi(x), x(0) \in K_0\} \tag{2}$$

which is a tube evolving under φ. The derivative of a tube $K(t)$ is denoted as $\overset{\circ}{K}(t)$, which, based on mutation analysis, must satisfy the following condition:

$$\lim_{\Delta t \to 0^+} \frac{1}{\Delta t} dh(K(t + \Delta t), T_\varphi(\Delta t, K(t))) = 0 \tag{3}$$

$$\overset{\circ}{K}(t) = \{\varphi(x) \in \mathrm{BL}(E, \mathbb{R}^n) \text{: (3) is satisfied}\}. \tag{4}$$

Therefore, the set dynamics mutation equation is defined as follows:

$$\varphi(x) \in \overset{\circ}{K}(t). \tag{5}$$

In addition, the controlled mutation equation (let U be the set of all the possible controls u) is defined as

$$\varphi(x(t), u(t)) \in \overset{\circ}{K}(t) \quad \text{with} \quad u(t) = \gamma(K(t)) \tag{6}$$

where φ: $E \times U \mapsto \mathrm{BL}(E, \mathbb{R}^n)$ is a mapping process from a state to a bounded Lipschitz function. γ: $2^{\mathbb{R}^n} \mapsto U$ is a feedback map from $K(t)$ to the control input.

B. Mutation Analysis for Scanning Probe Microscopy-Based Nanomanipulation

Mutation analysis provides an alternative way to solve a visual servoing problem: Design a controller $u(t) = \gamma(K(t))$ based on current image set $K(t)$ so that $dh(K(t), \hat{K}) \to 0$ as $t \to \infty$, where $K(0)$ and $\hat{K}$ are the initial (first current) and goal (desired) image sets, respectively.

In fact, if the function φ in (6) is linear in $u(t)$, we have the following theorem [17]: For the system described by mutation equation $L(x)u \in \overset{\circ}{K}(t)$ with $x \in \mathbb{R}^m$, $L(x) \in \mathbb{R}^{m\times n}$, $u \in \mathbb{R}^n$, and $K(t) \subset \mathbb{R}^m$, the following controller can locally exponentially stabilize the system at $\hat{K}$:

$$u(t) = \gamma(K) = -\alpha A(K)^+ V(K) \tag{7}$$

where $\alpha > 0$ is a gain factor. $A(K)^+$ is the Moore–Penrose pseudoinverse of $A(K) \in \mathbb{R}^{1\times n}$ defined by

$$A(K) = \int_K d^2_{\hat{K}}(x) \sum_{i=1}^{m} \frac{\partial L_i}{\partial x_i} dx + 2\int_K [x - \Pi_{\hat{K}}(x)]^{\mathrm{T}} L(x) dx - 2\int_{\hat{K}} [\hat{x} - \Pi_K(\hat{x})]^{\mathrm{T}} L(\Pi_K(\hat{x})) d\hat{x}$$

where L_i is the ith row vector in matrix L. $V(K)$ is the Lyapunov function defined as

$$V(K) = \int_K d^2_{\hat{K}}(x) dx + \int_{\hat{K}} d^2_K(\hat{x}) d\hat{x}. \tag{8}$$

The SPM performs imaging with two translational degree-of-freedom motion (vertical motion is used to obtain the sample topography). If the control input is $u = [u_x, u_y]^{\mathrm{T}}$, the mutation dynamic equation is

$$Lu \in \overset{\circ}{K}(t) \tag{9}$$

where

$$L = \begin{bmatrix} -1 & 0 \\ 0 & -1 \\ 0 & 0 \end{bmatrix}$$

is a constant matrix. Then, the controller can be obtained from (7):

$$u(t) = -\frac{\alpha}{2}\left\{ \int_K [x - \Pi_{\hat{K}}(x)]^{\mathrm{T}} L dx + \int_{\hat{K}} [\hat{x} - \Pi_K(\hat{x})]^{\mathrm{T}} L d\hat{x} \right\}^+ V(K). \tag{10}$$

III. Compressive Sensing for a Non-Vector Space Controller

In the non-vector space control system, SPM images are used as the feedback. The feedback image here is not the entire image, which takes too much time in scanning but is the local image whose dimension is much smaller. We developed a local scan strategy [3] to scan a small local area for its topography image; however, it still takes several seconds which is too slow to provide feedback for the non-vector space controller. To solve that, compressive sensing is used to reduce the time on scanning.

Considering an unknown signal $x \in \mathbb{R}^N$, if M linear measurements are taken according to a measurement matrix Φ (as shown in (11), in the case of $M = N$, the original signal x can be well sampled. However, we are more interested in the condition when $M \ll N$; fewer measurements might be enough to reconstruct the original signal.

$$y = \Phi x \tag{11}$$

where Φ is the measurement matrix, and $y \in \mathbb{R}^M$ is the measurement results. Equation (11) is an underdetermined equation if $M \ll N$. However, if adding some constraint such as that Φ has been properly designed and x is sparse, the unique solution of x can be found by solving the 0-norm minimization problem [23].

$$\hat{x} = \arg\min \|x\|_0 \quad \text{s.t.} \quad \Phi x = y. \tag{12}$$

Because solving the 0-norm minimization problem is NP-hard [24], [25], 1-norm minimization is used instead of 0-norm. Then, (12) could be written as

$$\hat{x} = \arg\min \|x\|_1 \quad \text{s.t.} \quad \Phi x = y \tag{13}$$

where $\hat{x}$ is the reconstructed signal.

Besides the 1-norm minimization algorithm, the minimization total variation method (14) is used for signal/image reconstruction. It can find the sparest solution in the intensity gradient level to obtain a continuous and smooth reconstructed image.

$$\hat{x} = \arg\min TV(x) \quad \text{s.t.} \quad \Phi x = y \tag{14}$$

where $TV(x) = \sum_{i,j} \sqrt{(x_{i+1,j} - x_{i,j})^2 + (x_{i,j+1} - x_{i,j})^2}$.

Because compressive sensing can reduce the number of measurements, it can be associated with local scan strategy to increase the feedback rate by further decreasing the scanning time. How to design a proper measurement matrix is a challenge for the implementation of compressive sensing into SPM. Usually, compressive sensing uses random measurement matrixes such as random Gaussian and Bernoulli matrixes. It is difficult to apply these random measurement matrixes to SPM due to the special working principle of SPM. The working principle of SPM is using a tip to scan on top of a sample surface, line by line, which is time-consuming work.

The measurement matrix in compressive sensing is an essential part due to the relationship between the measurement matrix and measurement efficiency. Following pestricted isometry property (RIP) [23] is a way to determine the sampling capability of a measurement matrix.

Definition 1: A matrix $A \in \mathbb{R}^{m\times n}$ satisfies the RIP condition of order S if there exists a $\delta_S \in (0, 1)$ such that

$$(1 - \delta_S)\|x\|_2^2 \le \|Ax\|_2^2 \le (1 + \delta_S)\|x\|_2^2 \tag{15}$$

for all the S sparse vectors $x \in \mathbb{R}^n$.

To test whether a matrix satisfies RIP condition is an exponential computational complexity problem. However, random matrices have been shown to satisfy the RIP condition with very

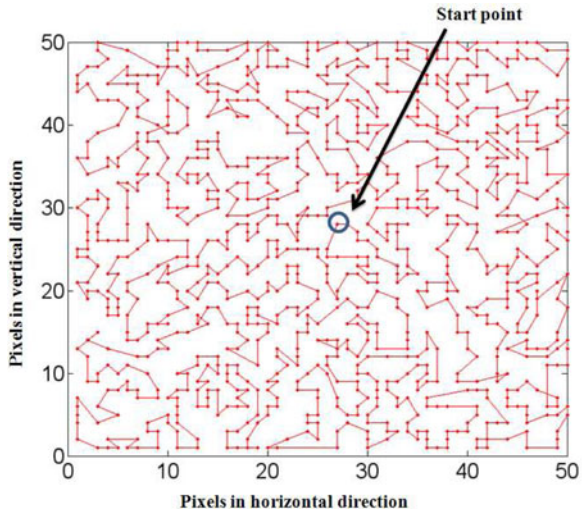

Fig. 3. Random sampling points and the TSP trajectory (800 random points in 50×50 points area with total travel distance 981.1645).

high probability. In order to design a random measurement matrix for SPM, the physical meaning of the measurement matrix in SPM imaging should be studied first. The tip scanning trajectory is determined by the measurement matrix. However, due to the imaging principle of SPM, a continuous trajectory should be found for random sampling points which can connect all the points with only one visit. This is a typical traveling salesman problem (TSP), which is an NP-hard problem. In order to find a near-optimal solution for this trajectory, the Genetic Algorithm (GA), which is a paradigm based on crossover and mutation, is used to solve this problem [26]. The working principle of this algorithm is that it connects each of the two points and then randomly selects the position to cut the connection between two points. Through the methods of recombination, mutation, and selection, the GA could search for new generation points which are better (shorter traveling distance) than the former trajectory. For example, we set the local area with 50×50 points, and after GA is applied, the trajectory obtained is shown in Fig. 3. The red line denotes the trajectory of the SPM tip which visits each point once and eventually returns to the initial point. If we assume that the distance between two neighboring points is one, the total travel distance is 981.1645. It is much shorter than raster scanning the entire local area (total distance is 2500). By means of compressive sensing, the control system can directly save the time spent on scanning which can increase the image feedback rate.

IV. Non-Vector Space Control Based on Compressive Feedback

Although compressive sensing decreases the time spent on scanning, it still needs extra time (approximate 0.5 s for 30×30 image) for image reconstruction. In order to further increase the feedback rate, we modified the non-vector space controller to use compressive feedback instead of complete image feedback directly. Although directly feeding back an image has avoided many difficulties associated with visual servoing such as feature extraction and extensive calibration, the amount of the data in feedback is large. It can significantly limit the feedback rate and require considerable computing power. The compressive feedback can solve this problem by significantly reducing the sampling and data transmission. As a matter of fact, the proposed compressive feedback makes the non-vector space control computationally feasible and efficient.

The derivation of a controller with compressive feedback is similar to the case of complete image based non-vector space control methodology which uses regular state feedback. The only difference from the approach in Section II is the type of feedback. The feedback for the former controller is a complete image recovered from compressive scanning. In contrast, for compressive feedback, the compressive data obtained by compressive scanning is used directly as the feedback without a recovery process, which increases the feedback rate. In other words, the SPM scanner only scans partial points of the local area. Based on this compressive data, a controller is designed to control the SPM's tip toward the desired position which is achievable if this process is performed repeatedly.

A. Controller Design

Because the mutation equation is the same and the compressive feedback (data) is also a set, the controller in Section II still works, and it can be slightly modified as follows.

Let K_c and $\hat{K}_c$ be the sets obtained by random scanning/sampling from the current and the desired image sets K, $\hat{K}$, respectively. The following controller can locally exponentially stabilize K_c at $\hat{K}_c$:

$$u(t) = -\frac{\alpha}{2}\left\{ \int_{K_c} [x - \Pi_{\hat{K}_c}(x)]^{\mathrm{T}} L dx + \int_{\hat{K}_c} [\hat{x} - \Pi_K(\hat{x})]^{\mathrm{T}} L d\hat{x} \right\}^{+} V(K_c) \tag{16}$$

where $V(K_c) = \int_{K_c} d^2_{\hat{K}_c}(x)dx + \int_{\hat{K}_c} d^2_{K_c}(\hat{x})d\hat{x}$.

This controller might not meet the goal of $dh(K, \hat{K}) \to 0$ as $t \to \infty$. There possibly exists another set $\widetilde{K}$ where $\hat{K}_c \subset \widetilde{K}$, if the cardinality of $\hat{K}_c$ is much less than that of $\hat{K}$. To prevent such a condition, we have to prove that when $dh(K_c, \hat{K}_c) \to 0$, $dh(K, \hat{K}) \to 0$, if K_c satisfies some certain constraints. These constraints come from the compressive sensing technique. Intuitively, there should be a unique K given a randomly subsampled $K_c \subset K$. Assume that the image is S sparse in the frequency domain (Fourier domain in this research, where the number of nonzero coefficients is S). If the image pixel intensity is sampled in a uniform random manner, the image can be exactly reconstructed by l_1 minimization algorithm in which the number of samples is of the order of $O(S \log^4 n)$.

B. Stability Analysis

Assume that the elements in set K are obtained from the image in order (for an image with $n \times n$ pixels, the first n elements in K are the first row (or column) of the image). Let

x_k be the kth vector of all the intensities of the image set K, and the elements in x_k are obtained using the same order in K. Let $\hat{x}_k$, x_{k_c}, and $\hat{x}_{k_c}$ be the vectors of the intensities of $\hat{K}$, K_c, and $\hat{K}_c$, respectively. The following lemma is used to prove the stability of the controller.

Lemma 1: $dh(K, \hat{K}) \to 0$ if and only if $\|x_k - \hat{x}_k\| \to 0$

Proof: 1) First of all, let us show $dh(K, \hat{K}) \to 0 \Rightarrow \|x_k - \hat{x}_k\| \to 0$. By the definition of Hausdorff distance, if $dh(K, \hat{K}) \to 0$, then for any $p = [p_1, p_2, p_3]^{\mathrm{T}}$ in set K, we have $\min_{q \in \hat{K}} \|p - q\| \to 0$. Let $q = [q_1, q_2, q_3]^{\mathrm{T}}$ be the element in $\hat{K}$ when the minimum is achieved, then $(p_1 - q_1)^2 + (p_2 - q_2)^2 + (p_3 - q_3)^2 \to 0$. Because the first two coordinates in p and q are the pixel indices, $(p_1 - q_1)^2 + (p_2 - q_2)^2$ cannot approach zero if the indices are different. Therefore, $p_1 = q_1$ and $p_2 = q_2$ which means the order of p and q are the same in K and $\hat{K}$, respectively. Moreover, we have $(p_3 - q_3)^2 \to 0$. Consequently, we have $\|x_k - \hat{x}_k\| \to 0$ since $\|x_k - \hat{x}_k\|^2$ is the sum of all the square of intensity differences for the same pixel indices such as $(p_3 - q_3)^2$.

2) Second, let us show $\|x_k - \hat{x}_k\| \to 0 \Rightarrow dh(K, \hat{K}) \to 0$. Let $p = [p_1, p_2, p_3]^{\mathrm{T}}$ in set K and $q = [q_1, q_2, q_3]^{\mathrm{T}}$ in set $\hat{K}$ be two arbitrarily elements with the same pixel indices, i.e., $p_1 = q_1$ and $p_2 = q_2$. Since $\|x_k - \hat{x}_k\| \to 0$, we have $(p_3 - q_3)^2 \to 0$. Then, for $p \in K$, we have $\min_{q' \in \hat{K}} \|p - q'\| \leq \|p - q\| \to 0$. For any other elements in K, we also have similar arguments. Therefore, $\max_{p' \in K} \min_{q' \in \hat{K}} \|p' - q'\| \to 0$. Similarly, we have $\max_{q' \in \hat{K}} \min_{p' \in K} \|q' - p'\| \to 0$. Therefore, $dh(K, \hat{K}) \to 0$. □

Besides the lemma, another equation, RIP condition (15) from the compressive sensing literature is used to establish the result. In fact, we have the following lemma:

Lemma 2 [27]: Let $\Phi \in \mathbb{R}^{n \times n}$ be the standard basis and $\Psi \in \mathbb{R}^{n \times n}$ be the Fourier basis. Then, the matrix $A = R\Phi\Psi^{-1}$ where $R \in \mathbb{R}^{m \times n}$ extracts m rows in $\Phi\Psi^{-1}$ uniformly in random. Then, A satisfies the RIP condition of order S with very high probability if $m \geq C \cdot S \cdot \log^4 n$, where C is a constant.

In order to verify the correctness of using compressive feedback, based on the above two lemmas, the following proposition is obtained.

Propsition 1: Assume $x_k \in \mathbb{R}^n$ and $\hat{x}_k \in \mathbb{R}^n$ are S sparse in the frequency domain, $x_{k_c} \in \mathbb{R}^m$ and $\hat{x}_{k_c} \in \mathbb{R}^m$ are obtained randomly from the image set K and $\hat{K}$. If $m \geq 2 \cdot C \cdot S \cdot \log^4 n$, where C is a constant. With high probability, we have $dh(K, \hat{K}) \to 0$ if $dh(K_c, \hat{K}_c) \to 0$.

Proof: From the random sampling, we have $x_{k_c} = Ax_k$ and $\hat{x}_{k_c} = A\hat{x}_k$. It is noted that based on the assumption, the random sampling matrix is the same as Lemma 2. Therefore, from Lemma 2, $A \in \mathbb{R}^{m \times n}$ satisfies the RIP condition with order $2S$. Let the RIP constant be δ_{2S}.

Using Lemma 1, we have $\|x_{k_c} - \hat{x}_{k_c}\| \to 0$ from $dh(K_c, \hat{K}_c) \to 0$. From the RIP condition, we have $\|x_{k_c} - \hat{x}_{k_c}\|_2^2 = \|Ax_k - A\hat{x}_k\|_2^2 \geq (1 - \delta_{2S})\|x_k - \hat{x}_k\|_2^2$. Since $1 - \delta_{2S} > 0$, we have $\|x_k - \hat{x}_k\| \to 0$. Based on Lemma 1 again, we have $dh(K, \hat{K}) \to 0$. □

The proposition shows that if certain conditions are satisfied, the same controller in (16) can be used under the compressive feedback.

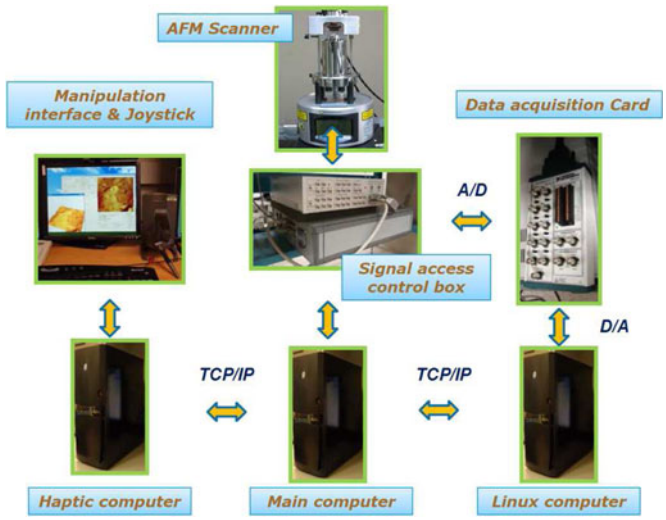

Fig. 4. Hardware architecture of the nanomanipulation system.

V. Experimental Implementation and Results

A. Experimental Implementation

In order to validate the non-vector space controller design and test the performance of this control system, it has been implemented into the AFM-based nanomanipulation system (as shown in Fig. 4). An AFM (Multimode, Bruker-nano, CA, USA) is used in this experiment. A computer with a haptic device, a real-time Linux system, and DAQ cards are used in this nanomanipulation system. In addition, a signal access and control box is developed to acquire the signal of topography information and input the control signal into the AFM controller.

B. Experimental Results of the Non-Vector Space Control With a Complete Image as Feedback

In this experiment, a conventional AFM was used to obtain an image of 1024×1024 pixels on a single-wall carbon nanotube (SWCNT) sample (scan size is 1.6 μm × 1.6 μm). This is the working area of the non-vector space controller. We named this AFM image "original image." Then, AFM scanned locally to get a small pitch image of current position. After that, a position close to the current position (approximately 56 nm away) was chosen as the desired position. The desired image can be easily selected in the original image. After calculations, the non-vector space controller provided the translational velocity u_x and u_y. The current and desired images, with a size of 30×30 pixels, are labeled in an original image in Fig. 5(a).

Results are shown in Fig. 5(b), where the iteration means the steps that AFM tip travels to the destination. At approximate 50 steps the AFM tip eventually reached the desired position when the distance approached zero. An additional note here is the error in a steady state. Theoretically, the error should converge to zero, as time goes to infinity; however, in AFM application, because of the thermal drift and noise, the non-vector space control has to continually minimize the error caused by the thermal drift and noise. This is the cause of the steady state error which is not zero in both the x and y directions.

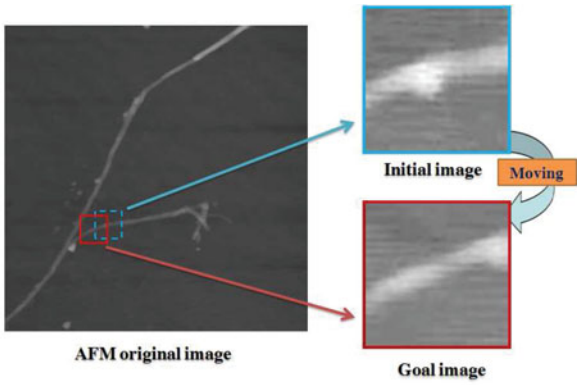

(a)

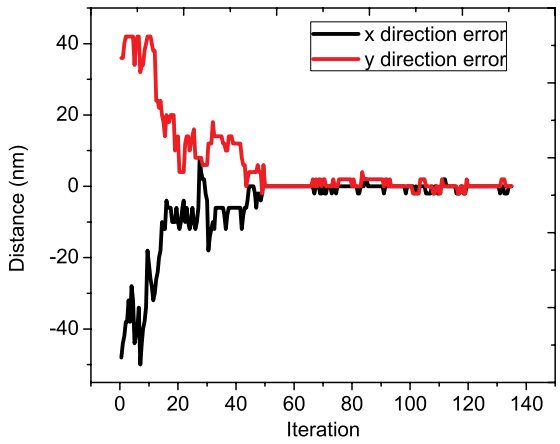

(b)

Fig. 5. Experimental setup and the results of a non-vector space control based on complete local images. (a) Experimental setup for the non-vector space control. (b) Experimental results of a non-vector space control with image as feedback: Error in the x and y directions.

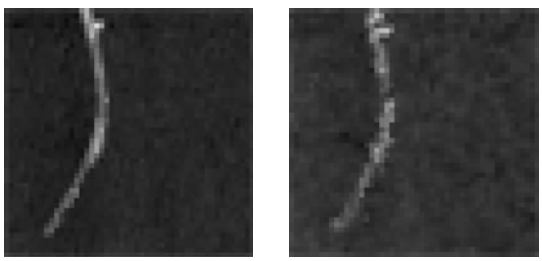

(a) (b)

Fig. 6. Experimental results of compressive sensing with random sampling. (a) Original AFM image on SWNT sample with 50×50 pixels. (b) Reconstructed image obtained by randomly compressive scanning on the same area.

C. Experimental Results of Compressive Sensing With Random Sampling

In the previous experiment, a non-vector space control system obtained the image feedback by scanning the entire local area which required extra time. In order to reach a higher sampling rate, imaging speed must be increased. Compressive sensing was utilized to solve this dilemma. The experimental results of compressive scanning and image reconstruction are shown in Fig. 6

These two images in Fig. 6 are 50×50 pixels and the scan size in each image is 1 μm × 1 μm of the SWCNT sample. After compressive sensing was applied, the scanning time decreased to 1.25 s (compared with 6.98 s in conventional raster scan). Compressive sensing can largely reduce the time spent scanning. However, for compressive sensing, it still requires time (approximately 1 s according to the TV-norm reconstruction method) to reconstruct the original image. In order to solve this new issue, the compressive sampling data are used as the feedback to the non-vector space controller directly without a reconstruction process.

D. Experimental Results of Compressive Feedback Non-Vector Space Controller

From the previous experiment, it is shown that compressive sensing could increase the sampling rate without losing important data information. However, its disadvantage is also obvious: Compressive sensing has to reconstruct the original image. The question is whether we can directly use the compressive data which is not an image but a set of random chosen data (compressive data) to serve as the feedback. In Section IV, the theoretical proof of this application was shown. In this section, an experiment was setup to test the performance of this control system. The experimental procedure is similar to the experiment in Section V-A. The only difference between these two experiments is that in this experiment the compressive data obtained by compressive scanning was used to replace the complete local image as the feedback. The same initial and desired locations as in the first experiment were used. The distance between the current position and desired position is 40 nm in the vertical direction and −41 nm in the horizontal direction. The feedback used in this experiment is a set of 350 elements [the ones inside 30×30 pixels as shown in Fig. 5(a)]. The experimental result is shown in Fig. 7(b). In this experiment, initial and desired positions are the same as the first experiment, but the calculation time spent on the compressive feedback controller (0.152 s) is much less than using the complete image as the feedback (0.322 s) in each step. That means the non-vector space controller based on the compressive feedback can reduce the time spent on both scanning and calculating.

E. Experiment on Tracking SWCNT-Based on the Compressive Feedback Non-Vector Space Controller

The goal of this example is using AFM tip to track along SWCNT. Before the start of the AFM tip motion control, first a high-resolution AFM image in the area of interest had been scanned as the original image [as shown in Fig. 8(a)]. The scan size of image is 1.25 μm × 1.25 μm, and the resolution is 1024×1024 pixels. Once the high-resolution image was obtained, the path-planner modules started working. The operator can select between two options: Automatically identify the SWCNT, and generate the tip path or manually design the arbitrary path. In this example, the path was selected manually by using the haptic device; the tracking path is shown in Fig. 8(b). Once the path was selected, the system automatically generated a sequence of images of the interim steps between start and end points [shown in Fig. 8(c)]. With the guidance of a non-vector

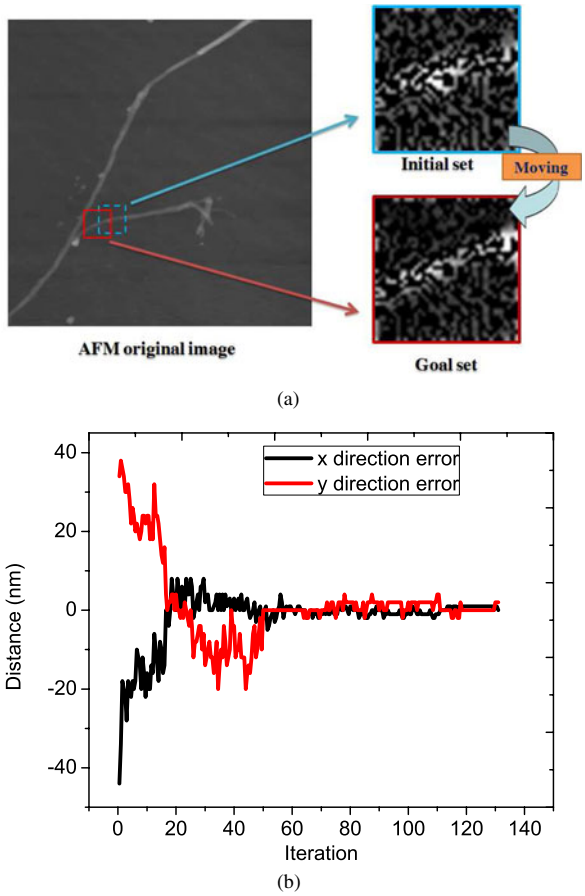

Fig. 7. Experiment setup and the results of a non-vector space control based on the compressive feedback. (a) Experimental setup for the non-vector space control based on the compressive feedback. (b) Experimental results of a non-vector space control with compressive feedback: error in x and y directions.

space controller, the AFM tip tracks the SWCNT and eventually reaches the goal position. In addition, the position error is shown in Fig. 8(d). The error is highly related to the image scan size and resolution. Generally, a smaller scan size with higher resolution will result in less position error. In order to achieve ultrahigh accuracy position and motion control, the scan size should be as small as possible. However, maintaining the proper image quality is a challenge when the scan size decreases into hundreds of nanometers, especially for the local image or compressed data used for the feedback. In this case, the noise in the image might influence the performance of the controller. The typical Hausdorff distance is very sensitive to the noise; therefore, in this application, the modified Hausdorff distance is used instead of a conventional Hausdorff distance. The modified Hausdorff distance is defined as follows.

Assuming a finite set of points $P \subset \mathbb{R}^n$, the distance between a point $x \in \mathbb{R}^n$ and the set is $d_P(x) = \min_{y \in P} \|y - x\|$. The modified Hausdorff distance (MHD) between two set P and Q is defined as [28]

$$dh(P,Q) = \max\left\{ \frac{1}{n} \sum_{p \in P} \min_{q \in Q} \|p - q\|, \frac{1}{n} \sum_{q \in Q} \min_{p \in P} \|q - p\| \right\}. \tag{17}$$

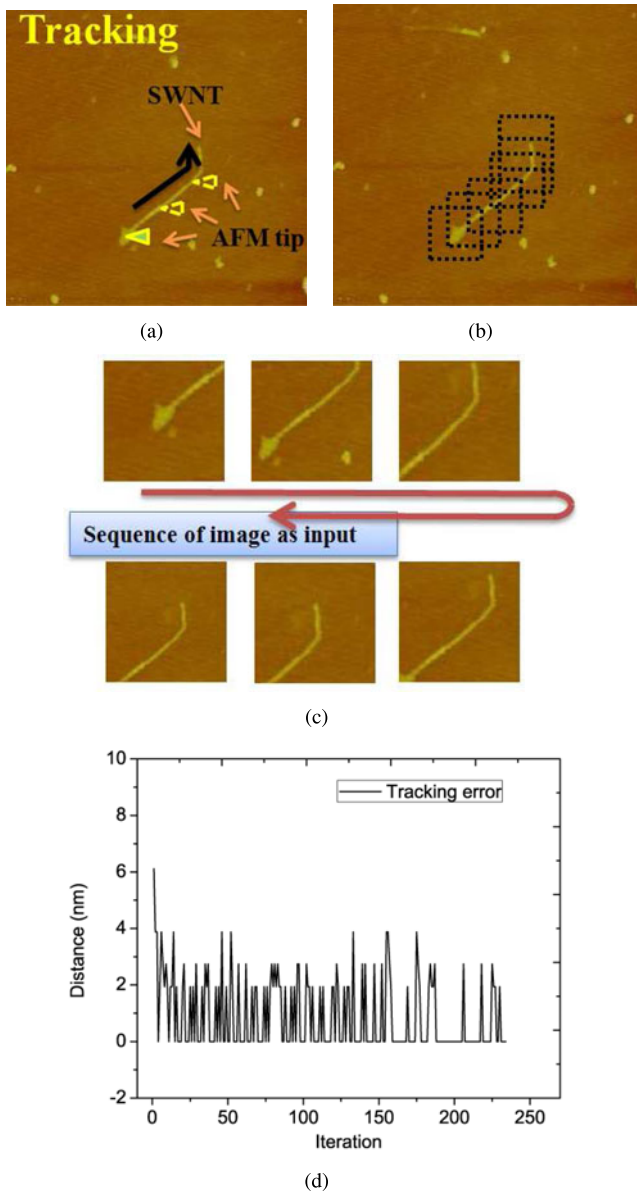

Fig. 8. Experimental results of tracking SWCNT using a non-vector space controller. (a) Original AFM image of 1024×1024 pixels. (b) Tracking path. (c) Sequence of images of the interim steps. (d) Position error during tracking.

The MHD is robust to the noise, which is suitable in this example. After MHD was applied into the non-vector space controller, the error range was controlled within 4 nm. The method to verify the position error in all experiments is the offline template matching. Because there is no position or displacement sensor in this open-loop AFM scanner, the way to calculate the absolute error is using each current local image as a template to match with an accurate position in the original image. This is the method to verify the error but not the one used in the non-vector space control strategy which used MHD to define the error between current and desired images.

F. Performance Analysis of Non-Vector Space Controllers

Currently, there are two different types of non-vector space controller—image feedback and compressive feedback. From

the experimental result, the steady-state error of the complete image feedback controller approaches zero (error is approximate ± 1 nm) in both the *x* and *y* directions, which proves that $dh(K(t), \hat{K}) \to 0$ as $t \to \infty$. However, in the case of compressive feedback, the error does not always converge to zero. This is because of the following proposition for the compressive feedback controller.

Proposition 1: Suppose both x and $\hat{x}$ obey the power law decay. Without loss of generality, assume that the largest $S = \lceil n/2 \rceil$ elements are used to approximate the original signals, where $\lceil \cdot \rceil$ is the ceil operator. If matrix A satisfies the RIP condition with order $2S$ and constant σ_{2S}, then $dh(K, \hat{K}) \leq 2R(\sqrt{1+\sigma_{2S}} + \sqrt{1-\sigma_{2S}})/\sqrt{S(1-\sigma_{2S})}$ if $dh(K_c, \hat{K}_c) \to 0$.

This proposition indicates that if $dh(K_c, \hat{K}_c) \to 0$, the set distance between the two compressive sets can be bounded. Therefore, instead of asymptotical stability, only the stability can be guaranteed (the detailed proof can be found in [29]). In other words, there exists a steady state error in the compressive feedback controller. As shown in Fig. 7(b), the steady-state error is approximately $\pm$2nm. Although the steady-state error exists in a compressive feedback controller, its reduced calculation time and high feedback rate are useful advantages for realtime control. It is noted that the accuracy of this non-vector space controller depends on the original image resolution and scan size which is used for visual servoing. If a 1024×1024 pixels AFM image with the scan size of 600 nm is used, the accuracy of this non-vector space control system will reach as high as 1 nm according to the experimental results.

In addition, theoretically, the initial image and goal image should be sufficiently close to each other (with some overlap). The "sufficiently close" comes from the local stability of the controller, which means the goal image should be in the vicinity of the initial image. The closeness can be described by the Hausdorff distance. The bound of the Hausdorff distance between the initial and goal image for successful control depends on the region of attraction of the controller. If the difference is too big for the controller to handle, a proper motion planner will be needed. In other words, instead of reaching the goal in one step, a trajectory will be planned to lead to the goal. Moreover, it might be possible that in certain areas, the controller may generate the same compressive feedback, and the output of the controller is the same. However, the next compressive feedback is unlikely to be identical to the previous compressive feedback (because of the random sampling and the fact that the surface is not perfectly periodic) and at that time, the controller can drive the tip toward the desired position.

VI. Non-Vector Space Control System Application: Carbon Nanotube Local Electrical Property Characterization

With the development of synthesis techniques of nanomaterials, including nanotubs, nanowires [30], nanopolymers [31], quantum wells and quantum dots [32], the electrical characterization of these materials, albeit more challenging, attracted strong attention. Nanomaterials have unique electrical properties due to quantum confinement. Not only do the electrical characterizations reveal the underlying physical, mechanical, and electrical properties of the nanomaterials, but they can also be utilized to fabricate high-performance sensors and devices, such as field-effect transistors (FETs) [33], [34], infrared sensors [35], gas sensors [36], and solar cells [37].

The conventional electrical characterization setup for nanotubes was measuring a global resistance by connecting a nanotube to two metals [38]. However, such a setup is only capable to measure the overall resistance of the devices, which cannot distinguish the conductance of contacts and nanomaterials. What is more, it lacks the capability to investigate the local conductance, which reflects underlying properties of the nanomaterials.

SPMs, which are conventional imaging tools with nanometer-resolution, have been proposed to study the local conductance of nanomaterials. They employed the conductive SPM probe as a movable electrode to conduct local conductance measurements [30], [39]–[41]. Despite the feasibility of this measurement technique, only a few attempts have been implemented, let alone the low reliability and resolution, because of the difficulties in accurate SPM tip motion and force control during the measurement. The experimental results of local conductance measurement from previous studies showed a large measurement variance [30], [41], and this was possibly due to inaccurate tip position control, which means that during the measurement, the conductive probe may not reach the desired measurement points. Next, the spatial resolution of measurement (typical 100 nm in traditional measurement methods) is not fine enough to investigate local electric properties at a nanoscale [40]. Additionally, contact resistance between conductive probe and nanowires is load-dependent [39]. In other words, in order to characterize the local conductance uniformly at each location, constant contact force should be maintained which is another difficulty in practice. The non-vector space control strategy has the potential to overcome these difficulties by improving the spatial resolution of probe motion control through which the position error can be controlled within several nanometers. In addition, the contact force between conductive probe and sample surface can be controlled by the force feedback system [42] and that ensures the constant contact resistance between the probe and sample. Therefore, the non-vector space control system has the potential to conduct delicate and complicated manipulation and measurement. In this section, we illustrate the efficiency of the non-vector control strategy by integrating the nanomanipulation with electrical characterization system to study local electrical property of a carbon nanotube.

A. Multiwall Carbon Nanotube (MWNT) Local Conductance Measurement

The carbon nanotube, which is a quasi-1-D material, has been used as a building block for a number of nanodevices. However, the electrical properties of the carbon nanotube are not fully understood. In particular, there are consistent controversies about the electron transport of a multiwall carbon nanotube (MWNT)

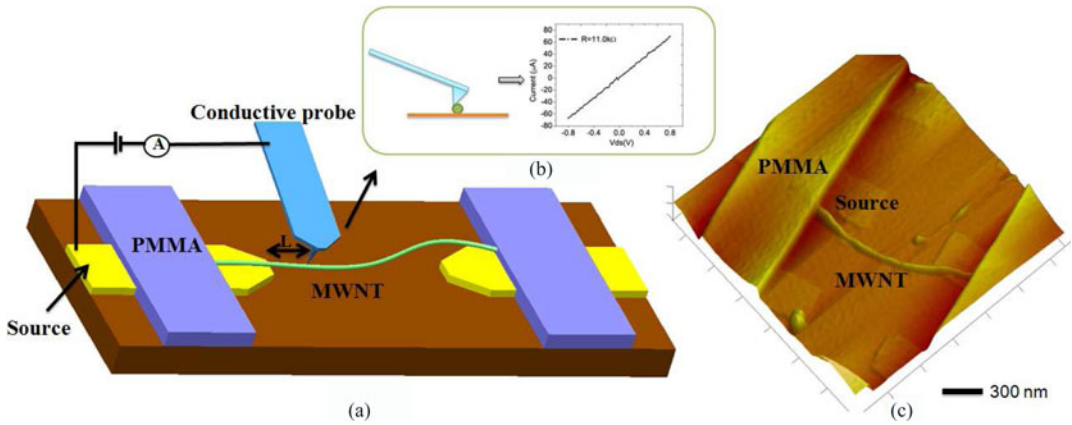

Fig. 9. Schematic diagram of experimental setup for characterizing local conductivity. (a) Experimental setup. (b) Using conductive tip to probe local conductance. (c) AFM image of testing sample: MWNT on Au-electrodes.

due to the complexity of inter- and intra-conductance. It is essential to understand the electronic properties of the material prior to designing a high-performance nanodevice. In this section, we use an AFM to investigate the local conductance of an MWNT as an example to illustrate the application of the non-vector space control mechanism.

The MWNT-based device is shown in Fig. 9(a) and (c). An MWNT bridges two metal electrodes on top of a Si/SiO2 substrate. The contacts between the MWNT and the metals were coated with two PMMA strips to clamp the MWNT on the substrate. One of the electrodes was connected to the ground as a source terminal; the conductive AFM tip acts as a drain electrode by physically contacting the MWNT during the measurement.

The fabrication process of the device started from fabricating two Au electrodes with a gap of 1 μm on the substrate through photolithography, thermal evaporation, and lift-off. It was followed by depositing an individual MWNT connecting two electrodes using dielectrophoresis (DEP) deposition system: MWNT powder, purchased from Bucky USA, was immersed into ethanol and ultrasonicated 10-20 minutes to form MWNT suspension; a droplet of the suspension was dispersed between the electrodes, and an AC voltage of 1 Vpp and 10 kHz frequency was applied to attract a MWNT to bridge the electrodes. A uniform PMMA layer was spin-coated on top of the device. The PMMA between two electrodes was removed after electron beam exposure and photoresist development, and two strips of the PMMA at the contacts were left to pin a MWNT on the substrate.

Before conducting local conductance measurement, the global I-V characteristics of the devices were measured by applying biases between the electrodes and recorded the current using a semiconductor analyzer. A metallic I-V characteristic was observed [as shown in Fig. 10(a)]. The total resistance of this MWNT is 11.0 kΩ. The samples were placed in an AFM (Dimension 3100, Bruker nano, CA) based compressive feedback based non-vector space nanomanipulation system integrating with an electrical measurement system. A diamond-coated conductive probe (DDESP-FM-10, Bruker nano, CA) was used as a movable drain electrode [as shown in Fig. 9(a) and (b)]. The channel length L is the distance from the conductive tip to the source electrode.

B. Measurement Results and Analysis

In this experiment setup, the length (L) dependent current (conductance) of the MWNT is measured with a length increment of 20 nm. The tip was first positioned above the MWNT at a specific location through a non-vector space controller, followed by lowering the tip until physically contact to the MWNT. The current flows between the conductive tip to the source electrode were recorded by a semiconductor analyzer. The resistance was plotted as a function of the channel length [as shown schematically in Fig. 10(b)]. The results show that the conductance of the MWNT was linearly dependent on the length, which reveal that 1) the contacts between MWNT and metal/tip are ohmic contacts instead of Schottky contacts and that 2) the electron transport is diffusive instead of ballistic in this sample. The results indicate that other local physical properties of the nanomaterials can also be investigated by changing the experimental conditions, for instance change the contact conditions, functionalize the MWNT using chemicals, etc.

Compared with the similar results from other researchers, our measurement method and result are more accurate and reliable. Additionally, it reveals more detailed information which is very essential for studying the local electrical properties. For example, the density distribution of measurement points is fairly high (20 nm interval between two measurement points) compared with hundreds nanometers interval in previous studies in this area. The most important, above all, is that the non-vector space controller can drive the conductive tip to precisely probe and measure every desired measurement point. That is impossible for convectional SPM manipulation, which is why the total resistance curve [see Fig. 10(b)] is linear with low variance that has never appeared in similar local conductivity research.

It should be noted that MWNT is just a single example. The AFM, integrating with the non-vector space control, may become a significant tool for the electrical characterization of all types of nanomaterial.

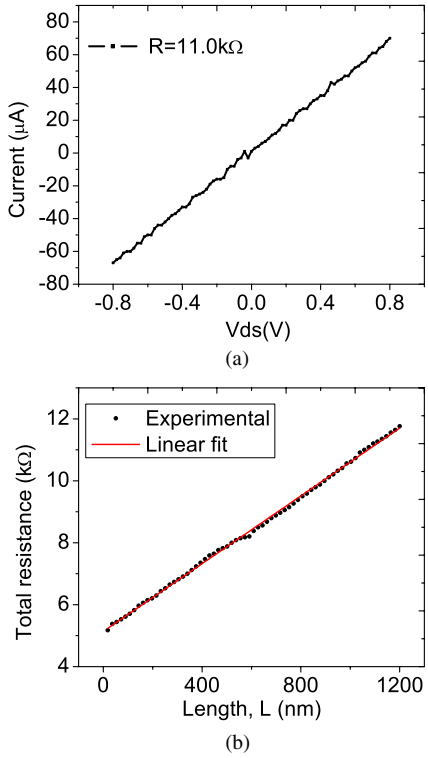

Fig. 10. MWNT electric property characteristics (a) *I–V* characteristics from source to drain electrodes. (b) Total resistance as a function of channel length.

VII. Conclusion

From a fundamental perspective, the non-vector space control method has the ability to make highly accurate SPM-based nanomanipulations easier. Besides, the compressive feedback can make a real-time nanomanipulation possible. The integration of these two approaches can achieve a high accuracy and high speed motion control for SPM-based nanomanipulation. Compared with the conventional vector space control method, the non-vector space control method gives a better performance (accuracy) in motion control that enables SPM to conduct more complicate and delicate nanomanipulations. This technique leads a new revolution to SPM-based nanomanipulation toward smaller, more accurate, and more reliable level. Moreover, this non-vector space control method is easy to implement into any kind of SPMs to realize a real-time control for nanomanipulation such as nanofabrication and nanoassembly.

Acknowledgment

The authors would like to thank Dr. C. Su of Bruker Nano Surface Instrumentation Group (former Veeco Instrument Inc.) for his technical advice and help during the process of this research.

References

[1] N. Xi, B. Song, R. Yang, K. W. C. Lai, H. Chen, C. Qu, and L. Chen, "Video rate atomic force microscopy: Use of compressive scanning for nanoscale video imaging," *IEEE Nanotechnol. Mag.*, vol. 7, no. 1, pp. 4–8, Mar. 2013.

[2] R. Yang, N. Xi, K. C. M. Fung, K. W. C. Lai, Seiffert-Sinha, and A. A. Sinha, "Analysis of keratinocytes stiffness after desmosome disruption using atomic force microscopy based nanomanipulation," in *Proc. IEEE Int. Conf. Nanotechnol.*, Genoa, Italy, 2009, pp. 640–643.

[3] B. Song, R. Yang, N. Xi, K. C. Patterson, C. Qu, and K. W. C. Lai, "Cellular-level surgery using nano robots," *J. Lab. Autom.*, vol. 17, no. 6, pp. 425–434, 2012.

[4] G. Li, N. Xi, M. Yu, and W.-K. Fung, "Development of augmented reality system for AFM-based nanomanipulation," *IEEE/ASME Trans. Mechatronics*, vol. 4, no. 9, pp. 358–365, Jun. 2004.

[5] R. V. Lapshin, "Analytical model for the approximation of hysteresis loop and its application to the scanning tunneling microscope," *Rev. Sci. Instrum.*, vol. 66, no. 9, pp. 4718–4730, 1995.

[6] R. V. Lapshin, "Automatic drift elimination in probe microscope images based on techniques of counter-scanning and topography feature recognition," *Meas. Sci. Technol.*, vol. 18, no. 3, pp. 907–927, 2007.

[7] P. Krejci and K. Kuhnen, "Inverse control of systems with hysteresis and creep," *Proc. Inst. Elect., Control Theory Appl.*, vol. 148, no. 3, pp. 185–192, May 2001.

[8] A. J. Fleming and K. K. Leang, "Integrated strain and force feedback for high-performance control of piezoelectric actuators," *Sens. Actuat. A, Phys.*, vol. 161, no. 1–2, pp. 256–265, 2010.

[9] Y. Zhu, S. O. R. Moheimani, and M. R. Yuce, "Simultaneous capacitive and electrothermal position sensing in a micromachined nanopositioner," *IEEE Electron Device Lett.*, vol. 32, no. 8, pp. 1146–1148, Aug. 2011.

[10] S. Gonda, T. Doi, T. Kurosawa, Y. Tanimura, N. Hisata, T. Yamagishi, H. Fujimoto, and H. Yukawa, "Real-time, interferometrically measuring atomic force microscope for direct calibration of standards," *Rev. Scientif. Instrum.*, vol. 70, no. 8, pp. 3362–3368, 1999.

[11] B. Song, J. Zhao, N. Xi, K. W. C. Lai, R. Yang, H. Chen, and C. Qu, "Non-vector space control for nanomanipulations based on compressive feedbacks," in *Proc. Robot. Autom. IEEE Int. Conf.*, 2012, pp. 2767–2772.

[12] F. Chaumette and S. Hutchinson, "Visual servo control—Part I: Basic approaches," *IEEE Robot. Autom. Mag.*, vol. 13, no. 4, pp. 82–90, Dec. 2006.

[13] E. Marchand and F. Chaumette, "Feature tracking for visual servoing purposes," *Robot. Auton. Syst.*, vol. 52, no. 1, pp. 53–70, 2005.

[14] C. Collewet and E. Marchand, "Photometric visual servoing," *IEEE Trans. Robot.*, vol. 27, no. 4, pp. 828–834, Aug. 2011.

[15] A. Dame and E. Marchand, "Mutual information-based visual servoing," *IEEE Trans. Robot.*, vol. 27, no. 5, pp. 958–969, Oct. 2011.

[16] L. Liu, Y. Luo, N. Xi, Y. Wang, J. Zhang, and G. Li, "Sensor referenced real-time videolization of atomic force microscopy for nanomanipulations," *IEEE/ASME Trans. Mechatronics*, vol. 13, no. 1, pp. 76–85, Feb. 2008.

[17] L. Doyen, "Mutational equations for shapes and vision-based control," *J. Math. Imag. Vis.*, vol. 5, no. 2, pp. 99–109, 1995.

[18] V. Kallem, M. Dewan, J. P. Swensen, G. D. Hager, and N. J. Cowan, "Kernel-based visual servoing," in *Proc. IEEE/RSJ Int. Conf. Intell. Robots Syst.*, San Diego, CA, USA, 2007, pp. 1975–1980.

[19] C. Collewet, E. Marchand, and F. Chaumette, "Visual servoing set free from image processing," in *Proc. IEEE Int. Conf. Robot. Autom.*, Pasadena, CA, USA, 2008, pp. 81–86.

[20] A. Dame and E. Marchand, "Improving mutual information-based visual servoing," in *Proc. IEEE Int. Conf. Robot. Autom.*, Anchorage, AK, USA, 2010, pp. 5531–5536.

[21] J. L. Barron, D. J. Fleet, and S. S. Beauchemin, "Performance of optical-flow techniques," *Int. J. Comput. Vis.*, vol. 12, no. 1, pp. 43–77, 1994.

[22] W. Rudin, *Principles of Mathematical Analysis*, 3rd ed. New York, NY, USA: McGraw-Hill, 1976.

[23] E. Candes, J. Romberg, and T. Tao, "Robust uncertainty principles: Exact signal reconstruction from highly incomplete frequency information," *IEEE Trans. Inf. Theory*, vol. 52, no. 2, pp. 489–509, Feb. 2006.

[24] D. L. Donoho, "For most large underdetermined systems of linear equations, the minimal l1 norm solution is also the sparsest solution," *Commun. Pure Appl. Math.*, vol. 59, no. 6, pp. 797–829, 2006.

[25] C. Hegde and R. G. Baraniuk, "Sampling and recovery of pulse streams," *IEEE Trans. Signal Process.*, vol. 59, no. 4, pp. 1505–1517, Apr. 2011.

[26] S. V. Ann, S. V. Ann, C. J. Yong, and C. J. Kiat, "Evolutionary algorithms for solving multi-objective travelling salesman problem," *Flexibile Serv. Manuf. J.*, vol. 23, no. 2, pp. 207–241, 2011.

[27] E. J. Candes and J. Romberg., "Sparsity and incoherence in compressive sampling," *Inverse Probl.*, vol. 23, no. 3, pp. 969–985, 2007.

[28] M.-P. Dubuisson and A. Jain, "A modified hausdorff distance for object matching," in *Proc. Pattern Recognit., 1994. Vol. 1—Conf. A: Comput. Vis. Amp; Image Process., Proc. 12th IAPR Int. Conf.*, vol. 1, pp. 566–568.

[29] J. Zhao, N. Xi, L. Sun, and B. Song, "Stability analysis of non-vector space control via compressive feedbacks," in *Proc. IEEE 51st Annu. Conf. Decis. Control*, 2012, pp. 5685–5690.
[30] Z. Fan and J. G. Lu, "Electrical properties of ZNO nanowire field effect transistors characterized with scanning probes," *Appl. Phys. Lett.*, vol. 86, no. 3, paper no. 032111, 3 pp., 2005.
[31] S. Desbief, N. Hergue, O. Douheret, M. Surin, P. Dubois, Y. Geerts, R. Lazzaroni, and P. Leclere, "Nanoscale investigation of the electrical properties in semiconductor polymer-carbon nanotube hybrid materials," *Nanoscale*, vol. 4, pp. 2705–2712, 2012.
[32] X. Michalet, F. Pinaud, L. Bentolila, J. Tsay, S. Doose, J. Li, G. Sundaresan, A. Wu, S. Gambhir, and S. Weiss, "Quantum dots for live cells, *in vivo* imaging, and diagnostics," *Science*, vol. 307, no. 5709, pp. 538–544, 2005.
[33] S. J. Tans, A. R. M. Verschueren, and C. Dekker, "Room-temperature transistor based on a single carbon nanotube," *Nature*, vol. 393, no. 6680, pp. 49–52, 1998.
[34] H. Z. Chen, N. Xi, K. W. C. Lai, L. L. Chen, R. G. Yang, and B. Song, "Gate dependent photo-responses of carbon nanotube field effect phototransistors," *Nanotechnol.*, vol. 23, no. 38, paper no. 385203, 8 pp.
[35] H. Chen, N. Xi, B. Song, L. Chen, J. Zhao, K. W. C. Lai, and R. Yang, "Infrared camera using a single nano-photodetector," *IEEE Sens. J.*, vol. 13, no. 3, pp. 949–958, Mar. 2013.
[36] Y.-J. Choi, I.-S. Hwang, J.-G. Park, K. J. Choi, J.-H. Park, and J.-H. Lee, "Novel fabrication of an SNO 2 nanowire gas sensor with high sensitivity," *Nanotechnol.*, vol. 19, no. 9, paper no. 095508, 4 pp., 2008.
[37] H. Chen, N. Xi, K. Lai, L. Chen, C. Fung, and J. Lou, "Plasmonic-resonant Bowtie antenna for carbon nanotube photodetectors," *Int. J. Opt.*, vol. 2012, paper no. 318104, 9 pp., 2012.
[38] H. Chen, N. Xi, K. Lai, C. Fung, and R. Yang, "Development of infrared detectors using single carbon-nanotube-based field-effect transistors," *IEEE Trans. Nanotechnol.*, vol. 9, no. 5, pp. 582–589, Sep. 2010.
[39] T. K. Ghanem, E. D. Williams, and M. S. Fuhrer, "Characterization of the electrical contact between a conductive atomic force microscope cantilever and a carbon nanotube," *J. Appl. Phys.*, vol. 110, no. 5, paper no. 054305, 7 pp., 2011.
[40] G. Jo, J. Maeng, T.-W. Kim, W.-K. Hong, B.-S. Choi, and T. Lee, "Channel-length and gate-bias dependence of contact resistance and mobility for in2o3 nanowire field effect transistors," *J. Appl. Phys.*, vol. 102, no. 8, paper no. 084508, 7 pp., 2007.
[41] X. Zhou, S. A. Dayeh, D. Aplin, D. Wang, and E. T. Yu, "Direct observation of ballistic and drift carrier transport regimes in inas nanowires," *Appl. Phys. Lett.*, vol. 89, no. 5, paper no. 053113, 3 pp., 2006.
[42] G. Li, N. Xi, H. Chen, C. Pomeroy, and M. Prokos, "videolized atomic force microscopy for interactive nanomanipulation and nanoassembly," *IEEE Trans. Nanotechnol.*, vol. 4, no. 5, pp. 605–615, Sep. 2005.

Bo Song (S'09) received the B.S. degree in mechanical engineering from the Dalian University of Technology, Dalian, China, in 2005 and the M.S. degree in electrical engineering from the University of Science and Technology of China, Hefei, China, in 2009. He is currently working toward the Ph.D. degree with the Department of Electrical and Computer Engineering, Michigan State University, East Lansing, MI, USA.

His current research interests include micro/nanorobotics and systems, micro/nanomanufacturing, nanomechanics, biomechanics, imaging and characterization in nano scale, and compressive sensing and control with limited information.

Jianguo Zhao (S'06) received the B.E. degree in mechanical engineering from the Harbin Institute of Technology, Harbin, China, in 2005 and the M.E. degree in mechatronic engineering from Shenzhen Graduate School, Harbin Institute of Technology, Shenzhen, China, in 2007. He is currently working toward the Ph.D. degree with the Robotics and Automation Lab, Michigan State University, East Lansing, MI, USA.

His research interests include bio-inspired robotics, dynamics and control, visual servoing, control with limited information, and cyber physical systems.

Ning Xi (F'07) received the D.Sc. degree in systems science and mathematics from Washington University in St. Louis, St. Louis, MO, USA in 1993 and the B.S. degree in electrical engineering from the Beijing University of Aeronautics and Astronautics, Beijing, China.

He is the University Distinguished Professor and John D. Ryder Professor of electrical and computer engineering with Michigan State University, East Lansing, MI, USA. He currently serves as the Head and the Chair Professor with the Department of Mechanical and Biomedical Engineering, City University of Hong Kong. His research interests include robotics, manufacturing automation, micro/nano manufacturing, nano sensors and devices, and intelligent control and systems.

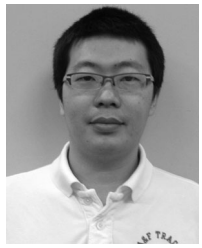

Hongzhi Chen (S'07) received the B.Eng. degree in information engineering from the Guangdong University of Technology, Guangzhou, China, in 2005 and the M.Sc. degree in electronics from Queen's University Belfast, Belfast, U.K., in 2006. He is currently working toward the Ph.D. degree with the Department of Electrical and Computer Engineering, Michigan State University, East Lansing, MI, USA.

His current research interests include nanoelectronics, nanophotonics, sensors, micro/nanofabrication and manufacturing, scanning probe microscopy, device characterization, MEMS/NEMS, and micro/nanorobotics and systems.

King Wai Chiu Lai (M'06) received the Ph.D. degree from the Department of Automation and Computer-Aided Engineering, Chinese University of Hong Kong, New Territories, Hong Kong, in 2005.

He joined Michigan State University, East Lansing, MI, USA, as a Postdoctoral Research Associate with the Department of Electrical and Computer Engineering in 2006. He is currently an Assistant Professor with the Department of Mechanical and Biomedical Engineering, City University of Hong Kong, Hong Kong. His main research interests include development of micro/nano sensors using MEMS and nanotechnology, nanobiotechnology, automation, and micro/nano manipulation.

Ruiguo Yang (S'08) received the B.S. degree in mechanical engineering and the M.S. degree in mechanical and electrical engineering from the Nanjing University of Aeronautics and Astronautics, Nanjing, China, in 2004 and 2007, respectively. He is currently working toward the Ph.D. degree with the Department of Electrical and Computer Engineering, Michigan State University, East Lansing, MI, USA.

His current research interests include nanomechanics, biomechanics, biomicroelectromechanical systems, biomedical imaging, characterization, and modeling.

Liangliang Chen received the Master and Bacherlor degree in electrical engineering from the Huazhong University of Science and Technology, Wuhan, China, in 2009 and 2007, respectively. He is currently working toward the Ph.D. degree with the Robotics and Automation Lab, Michigan State University, East Lansing, MI, USA.

His research interests include ultra weak signal detection in nano sensors, signal processing, analog circuits, and CNT nanosensors.